Hybrid constraint multi-line absorption spectroscopy for non-uniform thermochemical measurements in axisymmetric laminar and jet flames

Liuhao Ma [a,b,*], Kin-Pang Cheong [c,*], Kun Duan [b], Chaokai Yuan [d], Wei Ren [b]

[a] *Laboratory for Advanced Combustion, School of Automotive Engineering, Wuhan University of Technology, Wuhan, Hubei, China*
[b] *Department of Mechanical and Automation Engineering, and Shenzhen Research Institute, The Chinese University of Hong Kong, New Territories, Hong Kong SAR, China*
[c] *School of Aeronautics and Astronautics, Sichuan University, Chengdu, Sichuan, China*
[d] *State Key Laboratory of High Temperature Gas Dynamics, Institute of Mechanics, Chinese Academy of Sciences, Beijing, China*

ARTICLE INFO

ABSTRACT

We propose a novel strategy for the accurate determination of non-uniform thermochemical distributions in axisymmetric flames using line-of-sight laser absorption spectroscopy with the constraints of hybrid information. In this method, the computational fluid dynamics (CFD) simulation or other diagnostic method (e.g., thermocouple measurement) is used to qualitatively characterize the thermochemical properties, whereas the kinetic modelling, chemical equilibrium calculation and thermocouple measurement are used to constrain the range of unknown parameters. Experimental demonstrations were firstly performed in a standard laminar CH_4/air premixed flame stabilized on a McKenna burner at different equivalence ratios (Φ = 0.8-1.2). With proper hybrid constraints, multiple solutions are avoided, and the deviation and convergence time can be simultaneously reduced comparing to the conventional method. For further demonstration, this strategy was then applied to a turbulent jet flame to recover the significant thermochemical gradient without the need for tomographic reconstruction techniques.

1. Introduction

Laser absorption spectroscopy (LAS) is a powerful diagnostic technique for non-intrusive, species-specific, fast, quantitative and *in situ* measurements of multiple gas properties (i.e., chemical composition, temperature, pressure and velocity) [1–5]. This technique normally provides path-averaged results due to its line-of-sight (LOS) nature. However, in the actual combustion environments under open or confined conditions, significant thermochemical non-uniformities exist ubiquitously along the optical path due to complex chemical reactions, heat and mass transfers, shear and multiphase flows and other effects [6]. In combustion research, even for the widely-used lab-scale flat flames, there is only a limited uniform region under typical combustion conditions [7,8]. In the presence of the aforementioned thermochemical non-uniformity, the LOS measurement is prone to large errors [9]. Therefore, there is an urgent need for improving the capability of LOS LAS to quantitatively reconstruct the thermochemical parameters along the optical path in the non-uniform environment.

Many efforts have been devoted to reconstructing the non-uniform distribution along LOS in axisymmetric environments, including tomographic reconstruction [10–13] and multi-line thermometry [14–18]. The tomographic reconstruction method determines the non-uniform thermochemical distribution by combining multiple LOS measurements at different positions or directions with the Abel inversion method [19]. This method has been widely used for flame characterizations and successfully applied to practical propulsion engine exhaust measurements [20]. However, the implementation of this method requires many optical accesses, sophisticated optical setup, complex data processing and mathematical retrial methods.

Alternatively, multi-line thermometry resolves the non-uniform thermochemical distribution by exploiting the spectral information of multiple distinct absorption lines. It requires only a single LOS measurement across the center of the target field, which significantly simplifies the optical configuration and signal processing. By using the temperature-binning or profile-fitting strategy, thermochemical distributions can be obtained from the measured absorption spectrum [15–18]. Particularly, Liu et al. [15] performed the numerical and experimental research of the temperature-binning strategy to retrieve the non-uniform temperature distribution, which was further improved by adopting the regularization method [16]. Zhang et al. [17] explored the temperature non-uniformity using a combination of the binning strategy and Gauss-Seidel iteration methods. However, such a temperature-binning strategy becomes less efficient for complicated combustion fields. In the profile-fitting strategy, 2-T, parabolic, trapezoid and Boltzmann profiles are usually employed based on the prior knowledge of the combustion field [15,18].

---

* Corresponding authors.

E-mail addresses: liuhaoma@whut.edu.cn (L. Ma), kpcheong@scu.edu.cn (K.-P. Cheong).

For the simplest 2-T distribution, more than five absorption transitions are required to obtain reliable results [15]. In terms of the other distribution profiles such as trapezoid and Boltzmann profiles, the minimum number of required transitions increases to eight if no any physical constraints are considered. If a limited number of absorption lines are accessible, the profile-fitting strategy suffers from discrepant results. Additionally, the thermochemical distributions of turbulent flames cannot be simply described by 2-T, parabolic, trapezoid and Boltzmann profiles [3]. Although it is possible to describe the distribution by a piecewise function, there will exist a large number of unknowns, leading to multiple solutions, solutions with large deviations, or great computational cost for least-squares fitting.

In this work, we report the development of a hybrid constraint strategy for quantitative temperature measurements in non-uniform axisymmetric flames. A near-infrared diode laser at 1343 nm and a mid-infrared distributed feedback (DFB) laser at 2482 nm were used to exploit H_2O absorption lines, where temperature and H_2O concentration can be derived by a combination of the profile-fitting strategy and hybrid constraints from computational fluid dynamics (CFD) simulation, CHEMKIN kinetic modeling and thermocouple measurements. This technique was demonstrated for temperature and H_2O concentration measurements in both laminar and turbulent flames.

2. Spectroscopic fundamentals

The principle of LAS has been well documented in the literature [21]. Here we only briefly describe the spectroscopic fundamentals in the context of the current experiment to define the notation and clarify the proposed technique.

When a monochromatic and collimated laser beam at a specific frequency v (cm^{-1}) travels through the gas medium with an optical length of L (cm), the fractional transmission is governed by the Beer-Lambert law:

$$\alpha_v = -\ln\left(\frac{I_t}{I_o}\right)_v = k_v L = P \int_0^L S_i[T(x)]X_{abs}(x)\phi_v dx \tag{1}$$

where α_v and k_v represent the spectral absorbance and spectral absorption coefficient at optical frequency v (cm^{-1}), respectively, I_0 indicates the incident laser intensity, I_t indicates the transmitted laser intensity, P (atm) is the total gas pressure, $S_i[T(x)]$ (cm^{-2}·atm^{-1}) is the temperature-dependent line-strength of a particular ro-vibrational transition i, $T(x)$ and $X_{abs}(x)$ are the temperature and mole fraction of the absorbing gas at position x along the optical path, and ϕ_v (cm) is the normalized lineshape function. As ϕ_v is defined such that its integral over the entire optical frequency is unity, the integrated absorbance A_i is given by:

$$A_i = \int_{-\infty}^{\infty} \alpha_v dv = P \int_0^L S_i[T(x)]X_{abs}(x)dx \tag{2}$$

If the absorption information of multiple lines is obtained, the unknown variables can be obtained by solving the following non-linear equation set:

$$\begin{cases} A_1 = P \int_0^L X_{abs}(x)S_1[T(x)]dx \\ A_i = P \int_0^L X_{abs}(x)S_i[T(x)]dx \\ \vdots \\ A_m = P \int_0^L X_{abs}(x)S_m[T(x)]dx \end{cases} \tag{3}$$

The number of equations is normally larger than the number of unknown variables in thermochemical profiles so that the non-linear least-squares fitting (LSF) can be used to solve the Equation set (3) by:

$$\min_{T(x),X_{abs}(x)} \sum_{i=1}^{m} \left(\frac{P \int_0^L X_{abs}(x)S_i[T(x)]dx - A_{measured}^i}{A_{measured}^i} \right)^2 \tag{4}$$

As the range of temperature and gas concentrations are constrained by chemical equilibrium calculations (CEC), Eq. 4 can be expressed as

follows:

$$\min_{T(x),X_{abs}(x)} \sum_{i=1}^{m} \left(\frac{P \int_0^L X_{abs}(x)S_i[T(x)]dx - A_{measured}^i}{A_{measured}^i} \right)^2 \tag{5}$$
$$T_{max}(x) \leq T_{CEC}, X_{max}(x) \leq X_{CEC}$$

By further introducing the physical constraints from boundary conditions, the LSF can be replaced by the constraint least-squares fitting (CLSF) as:

$$\min_{T(x),X_{abs}(x)} \sum_{i=1}^{m} \left(\frac{P \int_0^L X_{abs}(x)S_i[T(x)]dx - A_{measured}^i}{A_{measured}^i} \right)^2 \tag{6}$$
$$T_{preheat\_zone} \leq T_{max}(x) \leq T_{CEC}, X_{preheat\_zone} \leq X_{max}(x) \leq X_{CEC}$$
$$T_{boundary}(L) \geq 300K, X_{boundary}(L) \geq 0$$

It often happens that there are not sufficient absorption lines to solve the unknown variables and that the proper thermochemical distribution is not always available. Thus, it may lead to the issue of multiple solutions or solutions with large deviations. Previous study found that a more appropriate distribution profile can contribute to a better retrieval of the thermochemical distribution [15]. Besides, prior knowledge of the target combustion field can help to constrain the number and range of the unknown variables.

Hence, in our proposed hybrid constraint least-squares fitting (HCLSF) method, we use the prior knowledge obtained from the CFD simulation to qualitatively predict the thermochemical distribution profile, which determines the number of unknowns preliminarily. Then we use the kinetic modeling and other sensors such as thermocouples to constrain the range of variables. The HCLSF can be treated as an information fusion-based technique to solve the following equation:

$$\min_{T(x),X_{abs}(x)} \sum_{i=1}^{m} \left(\frac{P \int_0^L X_{abs}(x)S_i[T(x)]dx - A_{measured}^i}{A_{measured}^i} \right)^2$$
$$\min\left\{ T_{TC}, T_{CHEMKIN}, T_{CFD} \right\} \leq T_{max}(x) \leq \max\left\{ T_{TC}, T_{CHEMKIN}, T_{CFD} \right\}$$
$$\min\left\{ X_{CHEMKIN}, X_{CFD} \right\} \leq X_{max}(x) \leq \max\left\{ X_{CHEMKIN}, X_{CFD}, X_{CEC} \right\}$$
$$300K \leq T_{boundary}(L) \leq \max\left\{ T_{TC}(L), T_{CFD}(L) \right\}$$
$$0 \leq X_{boundary}(L) \leq \max\left\{ X_{CFD}(L) \right\}$$
$$P_{constrained1} < Position_{Transition} < P_{constrained2}$$
$$G_{constrained1} < Gradient < G_{constrained2} \tag{7}$$

where $\min\{T_{TC}, T_{CHEMKIN}, T_{CFD}\}$ and $\max\{T_{TC}, T_{CHEMKIN}, T_{CFD}\}$ are the lower and upper limits of the thermocouple measurement, the CHEMKIN modeling, and the CFD simulation, respectively. A similar interpretation applies to $\min\{X_{CHEMKIN}, X_{CFD}\}$ and $\max\{X_{CHEMKIN}, X_{CFD}, X_{CEC}\}$. CEC indicates the chemical equilibrium calculation. The detailed thermochemical distribution function of the laminar premixed flames and the turbulent jet flames studied in this work can be found in the supplementary materials. For the laminar and jet flames, the "Position transition" means the radial position where the temperature/H_2O concentration are $(\beta_1 + \beta_2)/2$ and $(\beta_3 + \beta_4)/2$, respectively. The "Gradient" means the gradient of the temperature/H_2O concentration decline region. Taking the laminar flames for example, the upper limit of "Position transition" can't exceed the diameter of the flame (i.e., position near the flame edge), while the lower limit of "Position transition" is the position near the edge of central flame region. The upper and lower limits of "Gradient" are determined by the range of slope (the gradient from the position near the edge of central flame to the position near the flame edge).

Note that, the line selection is critical to obtain reliable measurements. The detailed line-selection criteria have been well documented in previous literature [14–16]. Following the well-validated criteria, seven absorption lines near 1343 and 2482 nm within the combination and fundamental band of H_2O are eventually selected. The spectroscopic parameters of the selected absorption lines can be found in the supplementary materials.
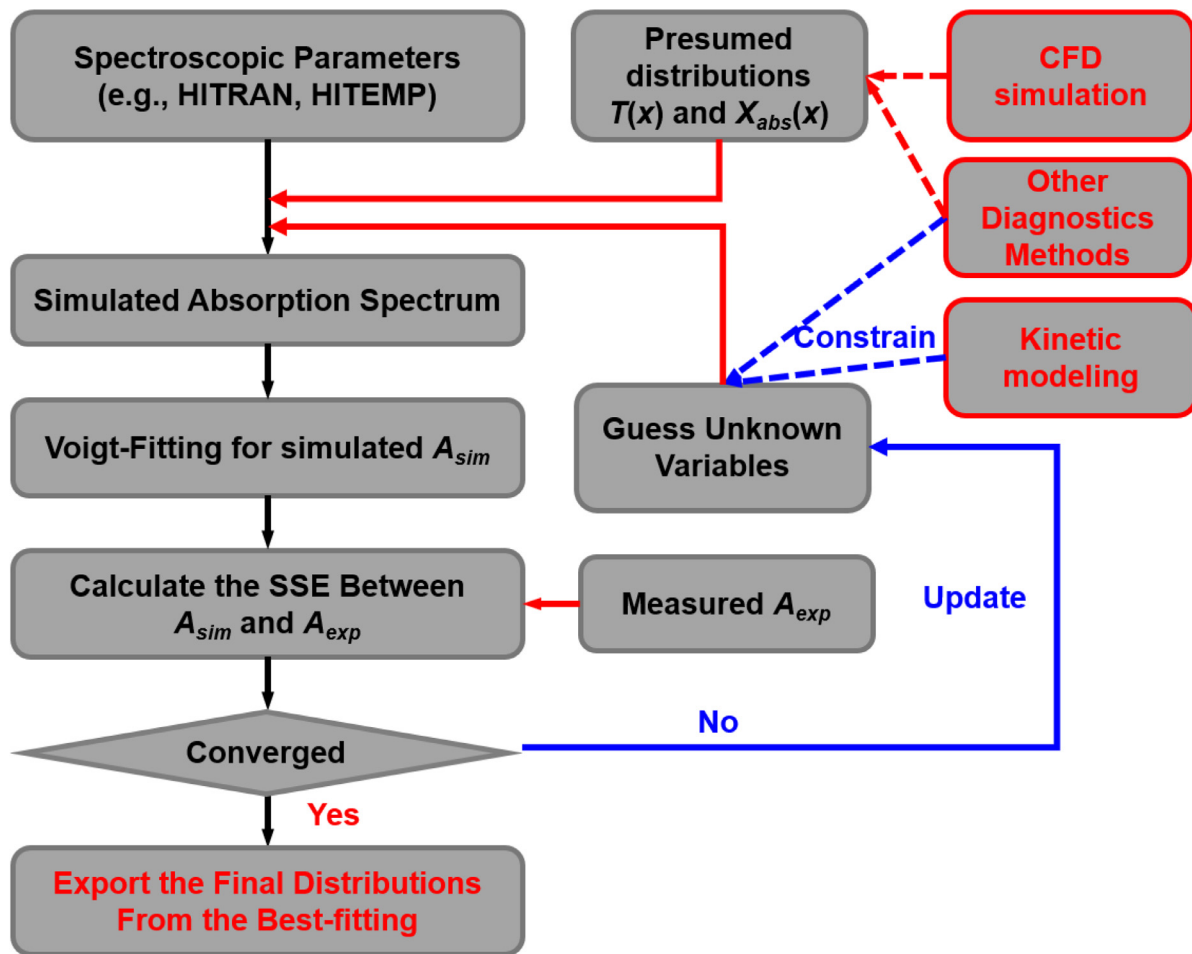
Fig. 1. Flow chart of the hybrid constraint least-squares fitting (HCLSF) method used for multi-line absorption spectroscopy.

Fig. 1 presents the flowchart of the diagnostic method. First, we can use kinetic modeling and other diagnostic methods (i.e., thermocouple) to constrain the range of variables and to reduce the number of unknown parameters. In laminar premixed flames on a McKenna burner, for instance, the CFD simulation of the laminar premixed flame reveals that the H_2O concentration and temperature have a similar distribution. Details of the CFD simulation and kinetic modeling can be found elsewhere [8,22,23]. Then the spectral simulation is performed based on the spectroscopic parameters, the presumed distributions of temperature and gas concentrations, and other presumed unknown parameters. By using the multi-Voigt fitting method of Levenverg-Marquardt (LM), the integrated absorbance of the selected absorption lines can be obtained. The sum-of-squared error (SSE) between the simulated integrated absorbance A_{sim} and the measured integrated absorbance A_{exp} is computed. The unknown variables are iteratively updated by enumeration until the SSE reaches the minimum.

3. Experimental

3.1. Flame description

The current study aims to demonstrate the feasibility of the HCLSF method for multi-line absorption measurements of non-uniform axisymmetric flames. Experiments were performed in a laminar premixed CH_4/air flame stabilized on a McKenna burner and a turbulent jet CH_4/air flame generated by a jet-in-hot-coflow (JHC) burner. The flame

structure and the three-dimensional rendering of the two burners are depicted in Fig. 2. All the laser absorption measurements were conducted at three HAB positions (HAB = 5, 10 and 15 mm for the laminar flame; HAB = 48, 72, 96 mm for the turbulent jet flame). For the laminar flames stabilized above the McKenna burner with a 60 mm-diameter sintered stainless-steel porous disk, the flow rate of reactant CH_4 was kept at 1.5 L/min, whereas the flow rate of oxidizer air was precisely adjusted between 12.0 and 18.0 L/min to acheive various equivalence ratios ($\Phi = 0.8$–1.2). The velocity of unburnt reactant mixtures varied from 0.080 m/s to 0.114 m/s, corresponding to Reynolds numbers of 297-432. The flow rate of co-flow nitrogen was fixed at 20 L/min as the shielding gas to achieve stable flames. Details of the McKenna burner and gas supply can be found elsewhere [18]. The JHC burner consists of a central jet (D = 1.2 mm) and an annular sintered copper (D = 99 mm). Coiled tubes are buried inside the sintered copper and wrapped around the sidewall for cooling. To achieve a more uniform and stable inlet velocity, glass beads are filled in the chamber under the sintered copper. The reactant mixture composition of the central jet was CH_4/air at $\Phi = 1.0$ and an unburnt temperature of 298.15 K. The bulk flow velocity was set to be 43.5 m/s, corresponding to a Reynolds number of ~3500. The premixed CH_4/air co-flow from the sintered copper has an equivalence ratio of $\Phi = 0.9$ and an unburnt exit velocity of 0.073 m/s. During the experiments, the premixed CH_4/air co-flow was firstly ignited to obtain a stable hot co-flow, then the central CH_4/air jet was introduced and ignited. More details of JHC burners are described elsewhere [23,24].
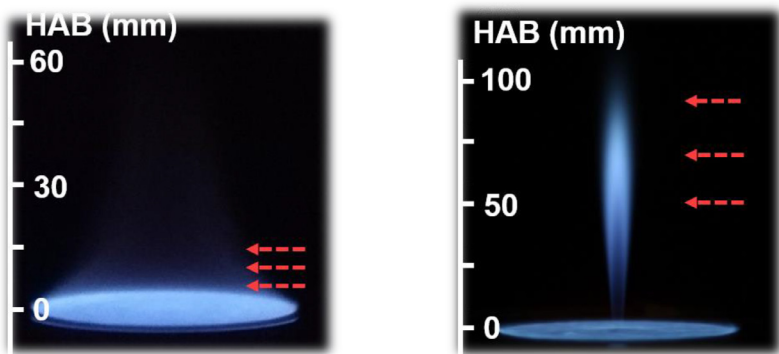
Fig. 2. (a) Laminar CH_4/air flame on a McKenna burner [25]; (b) turbulent CH_4/air jet flame on a JHC burner.
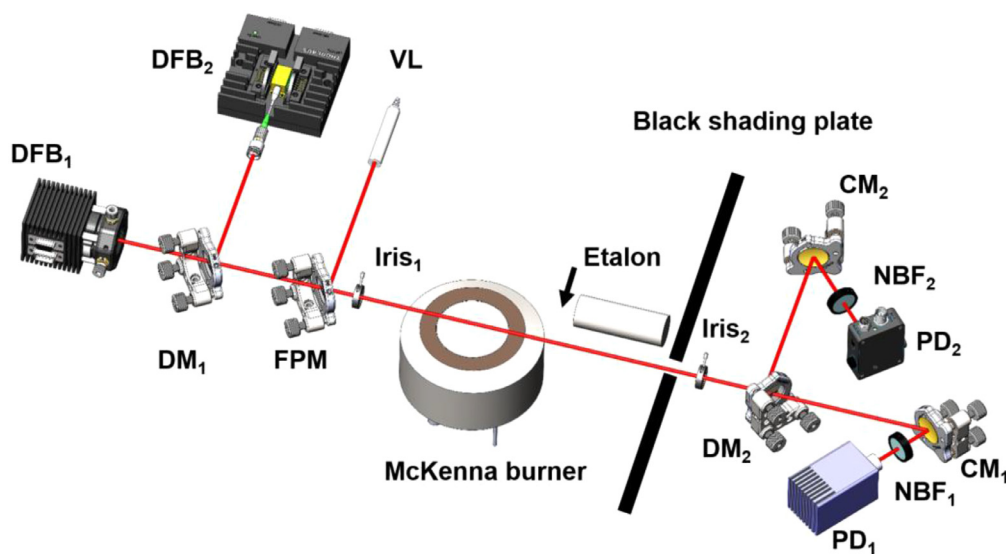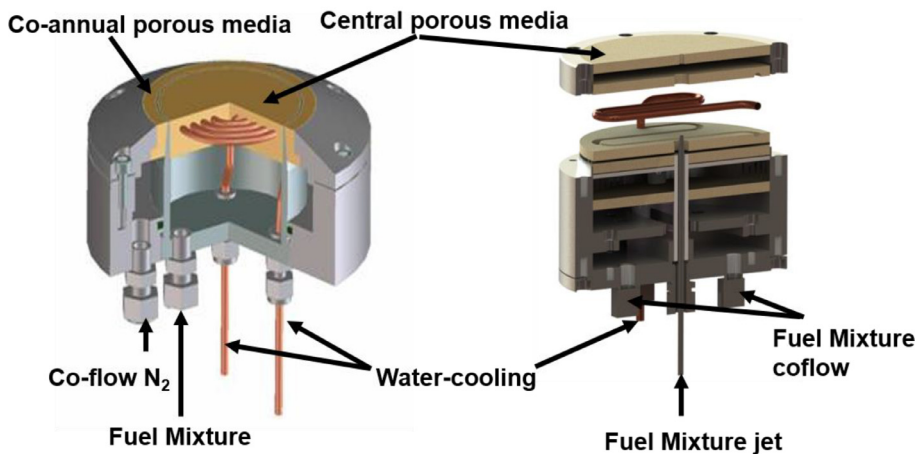

Fig. 3. Optical configuration of laser absorption diagnostics in the axisymmetric flame. DFB, distributed-feedback diode laser; VL, visible laser; PD, photodetector; DM, dichroic mirror; FPM, flipper plane mirror; CM, concave mirror; NBF, narrow-band-pass filter.

3.2. Optical setup

Fig. 3 depicts the schematic of the optical setup used for the present flame measurement. Two tunable continuous-wave distributed feedback (DFB) lasers at 2482 nm (Nanoplus GmbH) and 1343 nm (Nanjing Qingchen Inc.) were employed as the laser sources. The temperature and injection current of the two DFB lasers were controlled by the commercial low-noise laser drivers (Wavelength Electronics, LDTC 0520). The injection current was tuned to sweep across the selected H_2O transitions by a triangle signal generated using a function generator (TekTronix, AFG3052C). The scan rate was set to be 100 Hz for the laminar flame

and 1.6 kHz for the JHC turbulent flame to capture the temporal variance downstream. The laser beams were collimated by aspherical lens and orthogonally merged by a dichroic mirror (Thorlabs, DMSP1000) to pass through the flame. The transmitted laser beams were then separated by another dichroic mirror and collected by concave mirrors onto the photodetectors (Vigo Systems PVI-2TE-3; Thorlabs, PDA20CS2). To assist the optical alignment, a visible laser was used and made collinear with the two infrared lasers.

To minimize the influence of thermal radiation from the flame, two narrow bandpass filters (Spectrogon, NBF-2470-50; Thorlabs, FB1340-12) were placed in front of the photodetectors. A shading plate with a
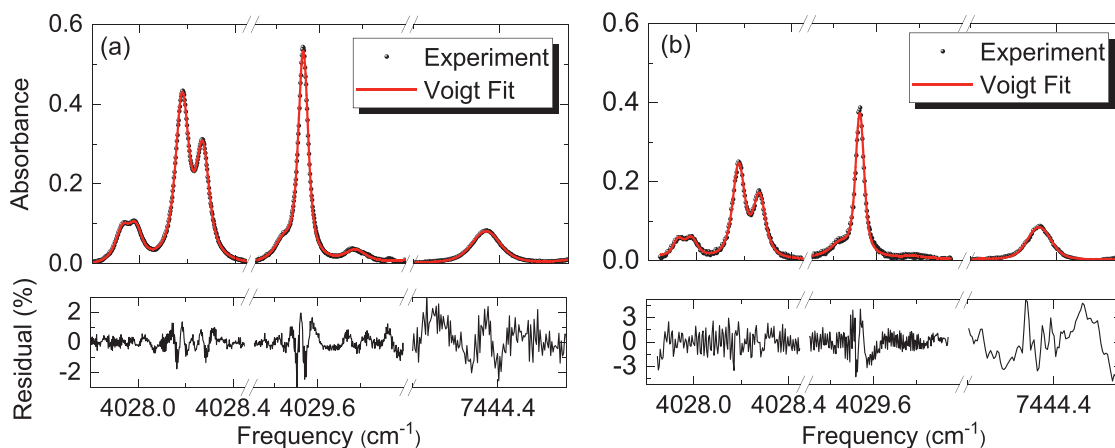
Fig. 4. Typical absorption spectra measured in (a) laminar premixed CH_4/air flame, and (b) turbulent CH_4/air jet flame. The fitting residual is plotted at the bottom panel.

2 mm hole was used to further mitigate the thermal radiation. Before each measurement, an etalon (FSR = 0.0164 cm^{-1}) was placed in the optical path for converting the scanning time to the relative frequency. As a benchmark for temperature measurement, a fine-wire B-type (Pt-30%Rh vs. Pt-6%Rh) thermocouple (Omega) with a diameter of 0.254 mm was used. The sampling interval of the thermocouple was 1 s and the mean temperature was obtained over 3 minutes with radiation and convection corrections (uncertainty ∼5.5%).

4. Results and discussion

4.1. Data analysis

Fig. 4 shows the representative measurement of the selected absorption spectra of H_2O along with the corresponding Voigt-fitting profiles. The fitting residuals over the entire spectrum for the laminar flame shown in Fig. 4(a) and the turbulent flame shown in Fig. 4(b) are within 3% and 5%, respectively. The overall measurement uncertainty of LAS was determined by a combination of the Voigt-fitting error (< 2%) of the integrated absorbance and the uncertainty of line-strength (< 2%). For example, when measuring the laminar CH_4/air flame at Φ = 1.0, we obtained the fitting residuals of 0.41%, (4028.178 cm^{-1}), 0.25 % (4028.256 cm^{-1}), 1.43% (4029.524 cm^{-1}), 0.78% (7444.360 cm^{-1}), respectively. Considering the uncertainty of line-strength (∼2.0%), we obtained a total uncertainty of 4.34% for the absorption measurement, leading to the temperature uncertainty of ∼82 K at the flame central temperature of 1882 K. The similar uncertainty analysis was applied to the measurement of the turbulent jet flame.

Fig. 5 compares the representative radial distributions of temperature and H_2O concentration, and the computational time using the LSF, CLSF and HCLSF methods. The term "HCLSF & LSF & CLSF" means that all the three methods can obtain the presented results, respectively. As multiple solutions are obtained using LSF or CLSF method, we mark the solutions as LSF 1, LSF 2, LSF 3, LSF 4, CLSF 1, CLSF 2 and CLSF 3. The LSF 1 and CLSF 1 are identical to the solution determined by HCLSF. Then the red solid curve in Fig. 5(a) corresponds to the solution marked as "HCLSF & LSF1 & CLSF 1". Similar explanation can be applied to the term "LSF & CLSF". The number "1-4" indicates the serial number of the multiple solutions. As shown in Fig. 5(a) and (b), the temperature and H_2O concentration obtained by HCLSF agree well with the thermocouple measurement and CFD simulation. Particularly, the central flame temperature obtained by the HCLSF method agrees well with the thermocouple measurement, CHEMKIN modeling and CFD simulation within 69 K (3.6 %). In comparison, the multiple solutions obtained by LSF show a larger deviation of the central flame temperature by 100 K (>

5.2%). The CLSF method can constrain the temperature range but still suffers from the issue of multiple solutions. In addition, we also compared the convergence time of LSF, CLSF and HCLSF methods as illustrated in Fig. 5(c). The convergence is defined that the sum-of-squared error (SSE) between the simulated integrated absorbance A_{sim} and the measured integrated absorbance A_{exp} reaches a minimum (10^{-5}-10^{-3}). The convergence time gradually decreases when more constraints are introduced during the iteration.

4.2. Laminar CH_4/air premixed flame

Thermochemical parameters in the central flame region are particularly important to the chemical kinetics study. Here we first discuss the measured central flame temperature and species compositions Fig. 6. summarizes the typical central temperature and H_2O concentration of CH_4/air flames at various equivalence ratios (Φ = 0.8-1.2). The measured LAS results are compared to the radiation-corrected thermocouple results, as well as the CFD and CHEMKIN simulations. The readers are referred to our previous work [8,22] for details of CFD and CHEMKIN simulation. The red shaded area and grey shaded area indicate the measurement uncertainties of LAS and thermocouple, respectively. The LAS-determined temperature agrees quite well with the thermocouple measurement within 20 K (< 1.1%). The CFD and CHEMKIN simulations also lie within the experimental uncertainty of LAS. Additionally, the LAS-determined H_2O concentrations are in excellent agreement with the CFD and CHEMKIN simulations; and the maximum absolute difference is only 0.3 % between LAS and CFD.

Fig. 7 depicts the representative radial distributions of temperature and H_2O concentration at different HABs and a fixed Φ = 1.0, along with the thermocouple measurements and CFD simulations. The shaded region in Fig. 7 designates the non-uniform flame with gradients temperature and species concentration. The LAS results are in good agreement with the thermocouple data and CFD results within the uniform region. The temperature and H_2O concentration gradients are captured relatively well by the LAS measurement with HCLSF.

4.3. Turbulent CH_4/air premixed flame

After the validation in laminar premixed flames, the LAS with HCLSF strategy was applied for studying the turbulent CH_4/air premixed jet flames Fig. 8. shows the representative time-resolved integrated absorbance of the two absorption lines centered at 4029.52 cm^{-1} and 7444.36 cm^{-1}, respectively, at three different HABs of the JHC. As shown in Fig. 8(a), the evident periodic behavior (7 Hz) of absorbance was observed in the 1-s time interval, which is mainly caused by the
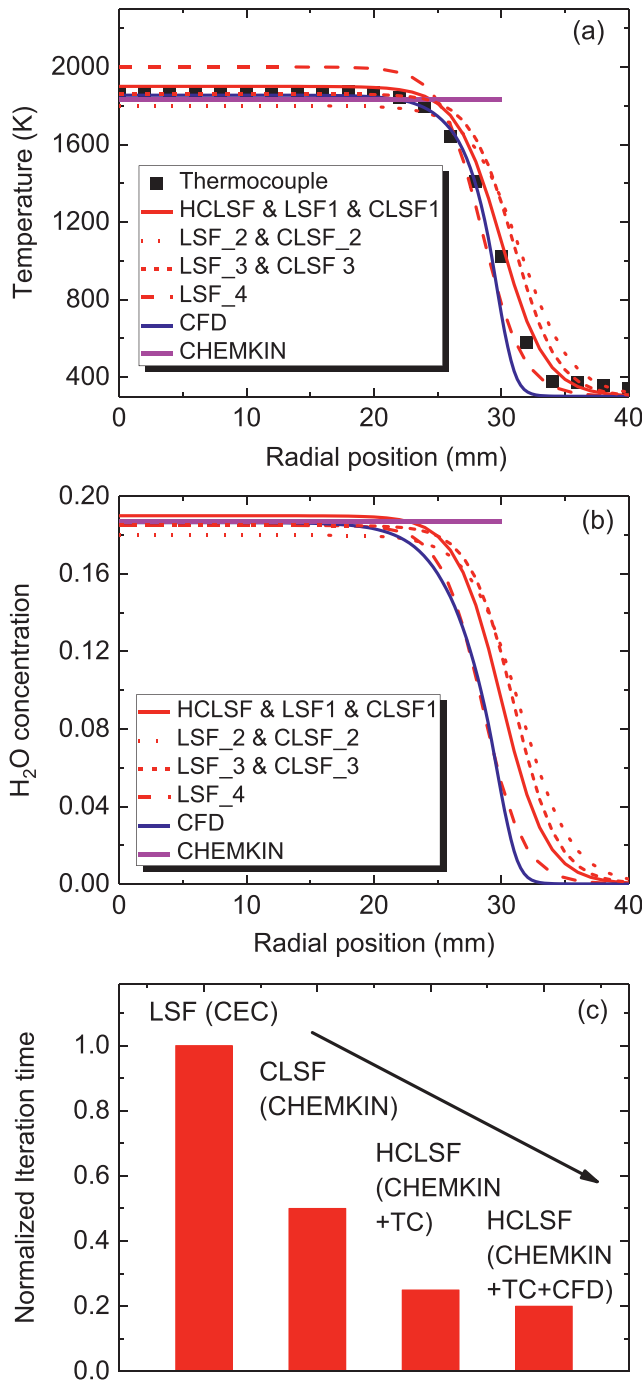
Fig. 6. Measured central flame temperature and H_2O concentration at HAB = 10 mm under different equivalence ratios (Φ = 0.8-1.2). Uncertainties of LAS and thermocouple measurements are shaded in red and grey, respectively.

Fig. 5. Representative radial distribution of (a) temperature, (b) H_2O concentration, and (c) the comparison of iteration time required for different LSF methods. The term "HCLSF & LSF & CLSF" in the legend means the distribution result is obtained from the three methods, respectively. The term "LSF & CLSF" in the legend means the distribution result is obtained from LSF and CLSF, respectively. LSF 1-4 means that the four results are obtained using the LSF method. CLSF 1-3 means that the three results are obtained using CLSF.

hot co-flow induced buoyancy instability. The spikes within the periodic signal include both the absorbance fluctuation caused by the turbulent instability and the experimental noise. The spike noise becomes more significant at higher HABs. This is because the flow becomes more turbulent due to the interactions between the central jet and hot co-flow, and the signal-to-noise ratio becomes lower due to the lower ab-
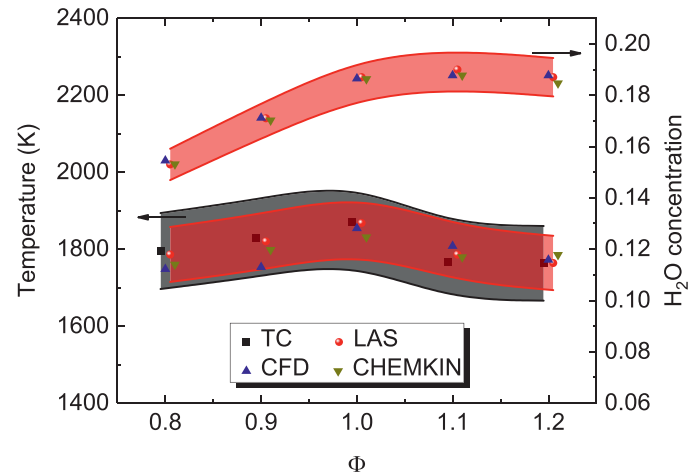
sorbance. However, at all three HABs, we are able to obtain relatively stable values of the averaged integrated absorbance over the 1 s interval, as illustrated in Fig. 8(b). Therefore, we can take an average of the measured integrated absorbance over a period of 30 s to represent the time-averaged result.

Fig. 9 presents the radial distributions of temperature measured at three different HABs. The LAS-determined temperature is in good agreement with the thermocouple measurement in terms of the central jet region and the hot co-flow region. More specifically, within the central jet region (red shaded region), the maximum temperature difference is ~4.6% existing at HAB = 48 mm, whereas the maximum temperature difference of 3.2% exists at HAB = 72 mm. Note that the central jet region expends radially as the flow goes downstream and the temperature profile of the jet region approaches a Gaussian distribution, which is the main feature of a fully developed turbulent jet [26]. In the hot co-flow region, the LAS measurement agrees well with the thermocouple measurement with a difference of 10–50 K. The LAS well captures the three-stage temperature variation from the central jet to the hot premixed co-flow and till the cool surroundings. The thermocouple measurement in the radial direction was stopped when it displayed unstable readings near the boundary region, where the temperature is < 450 K.

Similarly, the radial distribution of H_2O concentration was determined by the HCLSF shown in Fig. 10. The evident non-uniform distribution is observed from the central jet region to the hot coflow region. In addition, the measurement successfully captured the effect of air entrainment as the turbulent jet travels downstream, which can be interpreted from the decreasing H_2O concentration and peak temperature (Fig. 9) at higher HAB within the central jet region and hot coflow region.

Note that, local temperature and H_2O concentration (X_{H2O}) are highly correlated due to their common relevance to heat release or combustion reactions in flames [27]. In the turbulent flames, temperature and H_2O concentration are also statistically correlated in time. Pineda et al. performed the pioneering study of correlated variables effects on the LAS-determined thermochemical parameters and found there exists deviations in measuring the time-averaged variables in the presence of correlated fluctuations [28]. Following the similar method, the influence of turbulence-induced correlated fluctuations on temperature and H_2O concentration measurement in the current JHC flame was investigated. In the current multiline absorption spectroscopy, the correlated temperature and X_{H2O} fluctuations mainly cause fluctuations in the integrated absorbance A, making the time-averaged A deviates from the
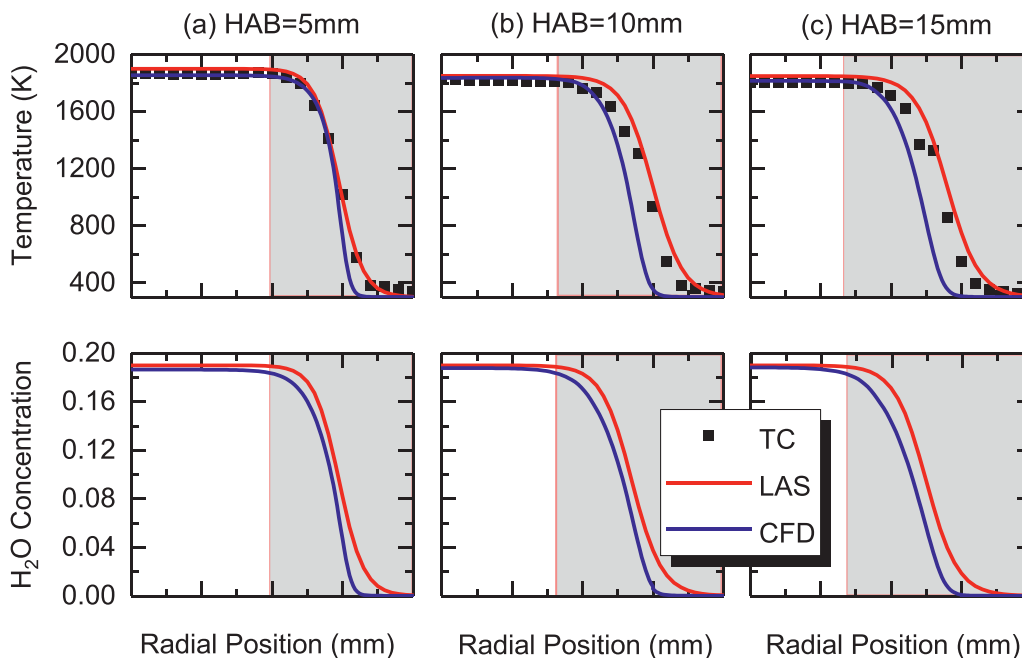
Fig. 7. Radial distribution of temperature and H_2O concentration at different HABs ($\Phi = 1.0$). Symbol: thermocouple measurement; red line: LAS measurement with HCLSF; blue line: CFD simulation.
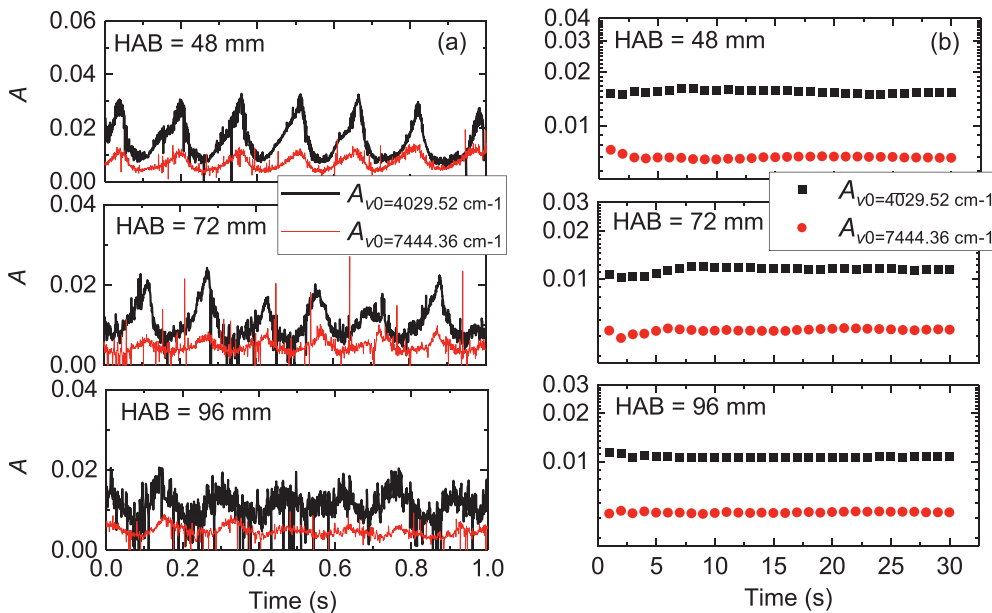

Fig. 8. Time-resolved integrated absorbance (A) of two absorption lines at 4029.52 cm^{-1} and 7444.36 cm^{-1}: (a) time-resolved measurement in 1 s; (b) averaged integrated absorbance in 30 s.

result obtained from the time-averaged spectrum, which can be mathematically expressed as $\overline{A_i(T(x), X_{abs}(x))} \neq A_i(\overline{T(x)}, \overline{X_{abs}(x)})$. The deviation can be expressed as "$\overline{A_i(T(x)', X_{abs}(x)')}$", which represents the time-averaged correlation between the turbulent fluctuations in temperature and X_{H2O}. $T(x)'$ and $X_{abs}(x)'$ denotes the fluctuation value of temperature and X_{H2O}. Note that, according to previous measurements in the turbulent jet flames by Rayleigh scattering, temperature and H_2O concentration are positively correlated [29]. The probability distribution function of the two parameters in the downstream follows Gaussian distribution. Therefore, we firstly performed a numerical study to investigate the turbulent fluctuations on the time-averaged temperature and H_2O. One hundred thousand (100,000) random numerical tests were

performed for flames with different turbulent intensity (TI). Note that, we fix the mean H_2O concentration at 0.15 to explore the fluctuation effects on the measured X_{H2O}. Firstly, we investigate the fluctuations effect on homogeneous environment with uniform temperature and X_{H2O}. The correlation between the temperature and species fluctuations has been set to 0.95. Fig. 11 depicts the correlated temperature and H_2O concentration as a function of set temperature along with the absolute difference under different turbulent levels. The schematic diagram of the fluctuated temperature and H_2O and the corresponding statistics histogram are included in Fig. 11(b). It can be figured out that the influence of correlated fluctuations has negligible influence on the measured temperature and X_{H2O} when the TI is relatively small (≤ 0.05). The ab-

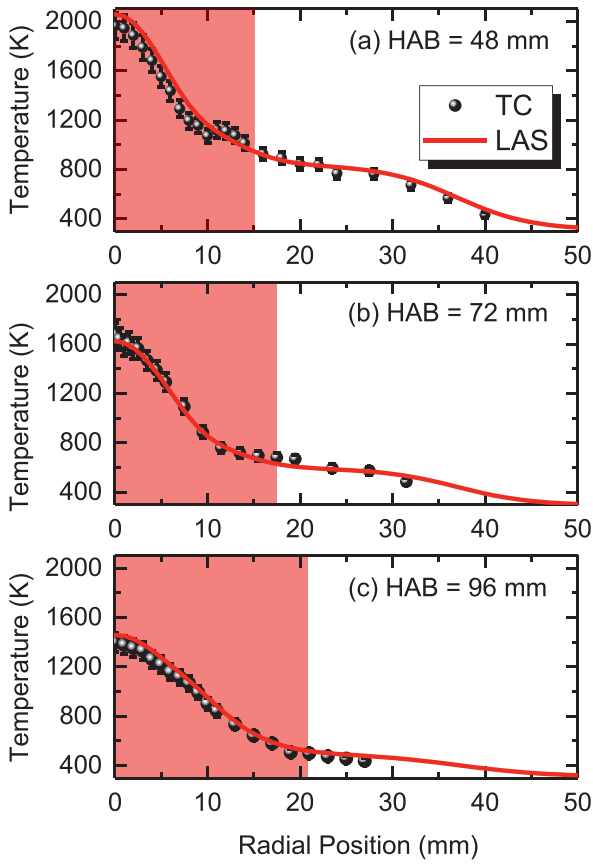**Fig. 9.** Radial distribution of temperature at various HABs: (a) HAB = 48 mm; (b) HAB = 72 mm; (c) HAB = 96 mm. Red shaded region: central jet region.

Fig. 10. Radial distribution of H_2O concentration at various HABs.

solute temperature difference is mostly within 45 K and the absolute H_2O concentration difference is within 0.4%.

For the radial distributions of temperature and H_2O concentration at various HABs in the current JHC flame, we have conducted similar numerical tests to local temperature and X_{H2O} following the method above to evaluate the effect of turbulence at different turbulent intensity. The fluctuation-induced deviations in the integrated absorbance A
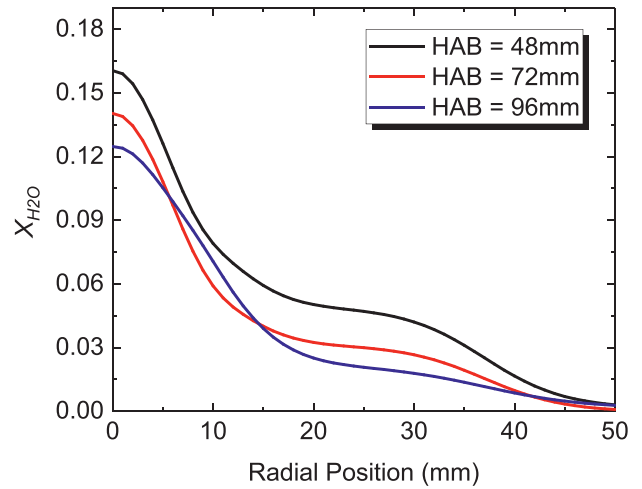
then affects the measurements of temperature and X_{H2O}. A representative summary of the influences on the measurements at HAB = 48 mm was presented in Fig. 12. The narrow shaded regions represent the fluctuation-induced uncertainties (statistical variations) when the effect of homogeneous turbulence is considered. It is clearly seen that turbulence of low turbulent intensity have limited impact on the temperature and H_2O concentration results when TI is small. For TI $\leq$ 0.05, the statistical uncertainties caused by the fluctuated combustion field on temperature and X_{H2O} are estimated to be less than 50 K and 0.5 %, respectively, which demonstrates the reliability of the present measurements.

Additionally, for the turbulent jet flame, CFD simulations were conducted before the experiment to identify the number of unknowns regarding the profile we proposed for both temperature and species concentration. In this stage, the CFD simulations does not necessarily quantitatively agree with the experimental measurement. After the number of unknowns is determined, we followed the HCLSF method validated in the laminar flame to obtain the final LAS measurement for the turbulent flame. As we can see from Fig. 9, the result from the hybrid-constrained method agrees well with the measurement by thermocouple, which further validated our new method. Therefore, the CFD simulation does not necessarily served as a precise constrain for the present method but can
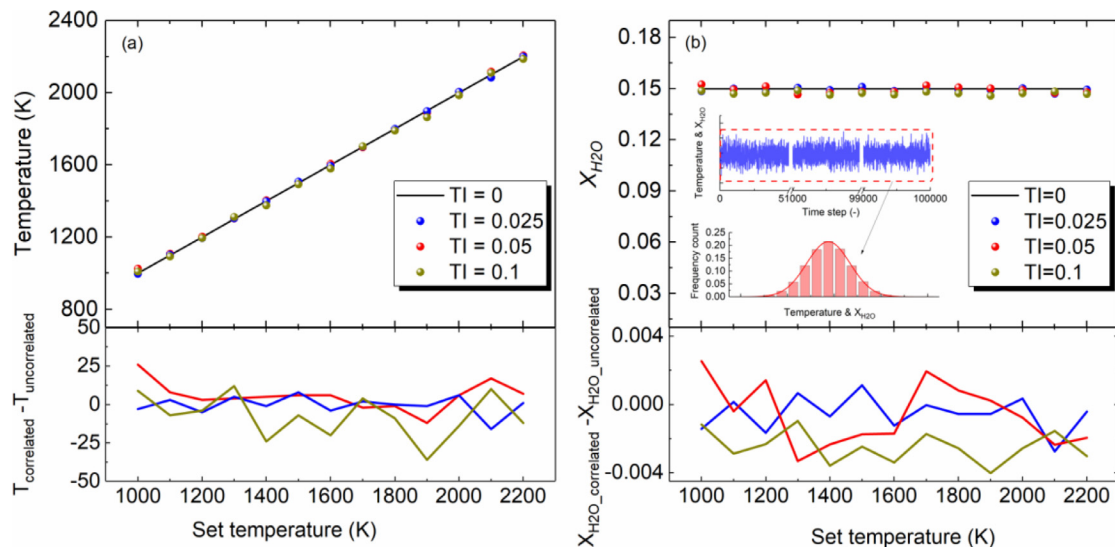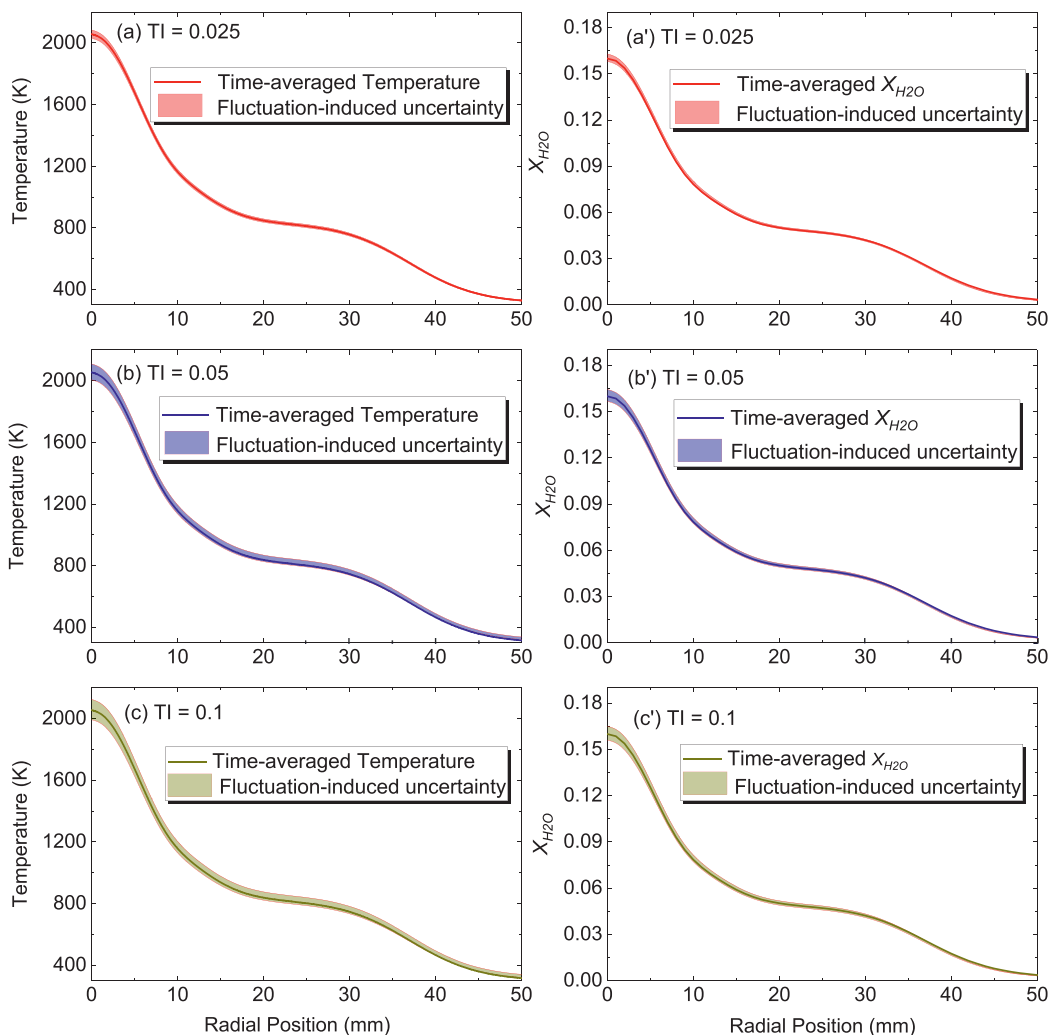

Fig. 11. Correlated temperature (a) and H_2O concentration (b) under different turbulent intensities.

Fig. 12. The radial distribution of temperature and H_2O concentration along with the fluctuation-induced uncertainty at HAB =48 mm under different turbulence intensity.

be a qualitative prior constrain when determining the form of profile distributions.

5. Conclusions

In this work, we developed a constrained strategy for quantitative measurements of non-uniform thermochemical distributions in axisymmetric flames based on line-of-sight laser absorption measurements. This strategy utilized the hybrid constraint information from numerical simulations or experimental measurements to avoid multiple solutions and accelerate convergence time during the least-squares fitting process. The proposed strategy was firstly demonstrated in a laminar CH_4/air premixed flame. The LAS measurements were compared to radiation-corrected thermocouple measurements, kinetic modelling and CFD simulations. Excellent agreement was observed for the central flame temperature and H_2O concentrations. For flame at $\Phi = 1.0$, the derived thermochemical distributions at different HABs agree well with the thermocouple measurements and CFD simulations. The proposed HCLSF method avoids the multiple solution problem even using less absorption transitions, meawhile significantly reduces the convergence time. Finally, the HCLSF method was also further demonstrated for the temperature and H_2O concentration measurements in turbulent jet flame. The radial distribution of temperature from high-temperature central jet region to hot coflow region was in good agreement with the thermo-

couple measurements. The HCLSF method proves to be a robust method with great potential for measuring flames with significant thermochemical non-uniformity.

Declaration of Competing Interest

The authors declare that they have no known competing financial interests or personal relationships that could have appeared to influence the work reported in this paper.

CRediT authorship contribution statement

Liuhao Ma: Conceptualization, Methodology, Investigation, Formal analysis, Visualization, Writing – original draft. **Kin-Pang Cheong:** Methodology, Investigation, Writing – review & editing. **Kun Duan:** Investigation, Writing – review & editing. **Chaokai Yuan:** Methodology, Investigation, Formal analysis. **Wei Ren:** Conceptualization, Investigation, Writing – review & editing, Supervision.

Acknowledgements

Supplementary materials

Supplementary material associated with this article can be found, in the online version, at doi:10.1016/j.optlaseng.2022.107014.

References

[1] Hanson RK. Applications of quantitative laser sensors to kinetics, propulsion and practical energy systems. Proc Combust Inst 2011;33:1–40.

[2] Goldenstein CS, Spearrin RM, Jeffries JB, Hanson RK. Infrared laser-absorption sensing for combustion gases. Prog Energy Combust Sci 2017;60:132–76.

[3] Liu C, Xu L. Laser absorption spectroscopy for combustion diagnosis in reactive flows: A review. Appl Spectrosc Rev 2019;54:1–44.

[4] Willer U, Saraji M, Khorsandi A, Geiser P, Schade W. Near- and mid-infrared laser monitoring of industrial processes, environment and security applications. Opt Lasers Eng 2006;44:699–710.

[5] Werle P, Slemr F, Maurer K, Kormann R, Mücke R, Jänker B. Near- and mid-infrared laser-optical sensors for gas analysis. Opt Lasers Eng 2002;37:101–14.

[6] Liu X. Line-of-sight absorption of H_2O vapor gas temperature sensing in uniform and nonuniform flows. Stanford, CA: Stanford University; 2006.

[7] Konnov A, Riemeijer R, Kornilov V, de Goey L. 2D effects in laminar premixed flames stabilized on a flat flame burner. Exp Therm Fluid Sci 2013;47:213–23.

[8] Ma L, Cheong K-P, Ning H, Ren W. An improved study of the uniformity of laminar premixed flames using laser absorption spectroscopy and CFD simulation. Exp Therm Fluid Sci 2020;112:110013.

[9] Qu Z, Werhahn O, Ebert V. Thermal boundary layer effects on line-of-sight tunable diode laser absorption spectroscopy (TDLAS) gas concentration measurements. Appl Spectrosc 2018;72:853–62.

[10] Nau P, Koppmann J, Lackner A, Kohse-Höinghaus K, Brockhinke A. Quantum cascade laser-based MIR spectrometer for the determination of CO and CO_2 concentrations and temperature in flames. Appl Phys B 2015;118:361–8.

[11] Xia H, Kan R, Xu Z, He Y, Liu J, Chen B, et al. Two-step tomographic reconstructions of temperature and species concentration in a flame based on laser absorption measurements with a rotation platform. Opt Lasers Eng 2017;90:10–18.

[12] Liu X, Zhang G, Huang Y, Wang Y, Qi F. Two-dimensional temperature and carbon dioxide concentration profiles in atmospheric laminar diffusion flames measured by mid-infrared direct absorption spectroscopy at 4.2 μm. Appl Phys B 2018;124:61.

[13] Wei C, Pineda DI, Paxton L, Egolfopoulos FN, Spearrin RM. Mid-infrared laser absorption tomography for quantitative 2D thermochemistry measurements in premixed jet flames. Appl Phys B 2018;124:123.

[14] Sanders ST, Wang J, Jeffries JB, Hanson RK. Diode-laser absorption sensor for line-of-sight gas temperature distributions. Appl Opt 2001;40:4404–15.

[15] Liu X, Jeffries JB, Hanson RK. Measurement of non-uniform temperature distributions using line-of-sight absorption spectroscopy. AIAA J 2007;45:411–19.

[16] Liu C, Xu L, Cao Z. Measurement of nonuniform temperature and concentration distributions by combining line-of-sight tunable diode laser absorption spectroscopy with regularization methods. Appl Opt 2013;52:4827–42.

[17] Zhang G, Liu J, Xu Z, He Y, Kan R. Characterization of temperature non-uniformity over a premixed CH_4–air flame based on line-of-sight TDLAS. Appl Phys B 2016;122:3.

[18] Ma LH, Lau LY, Ren W. Non-uniform temperature and species concentration measurements in a laminar flame using multi-band infrared absorption spectroscopy. Appl Phys B 2017;123:83.

[19] Cai W, Kaminski CF. Tomographic absorption spectroscopy for the study of gas dynamics and reactive flows. Prog Energy Combust Sci 2017;59:1–31.

[20] Ma L, Li X, Sanders ST, Caswell AW, Roy S, Plemmons DH, et al. 50-kHz-rate 2D imaging of temperature and H_2O concentration at the exhaust plane of a J85 engine using hyperspectral tomography. Opt Express 2013;21:1152–62.

[21] Hanson RK, Spearrin RM, Goldenstein CS. Spectroscopy and optical diagnostics for gases. Springer; 2016.

[22] Ma L, Ning H, Wu J, Ren W. In situ flame temperature measurements using a mid-Infrared two-line H_2O laser-absorption thermometry. Combust Sci Technol 2018;190:393–408.

[23] Wang F, Li P, Mi J, Wang J, Xu M. Chemical kinetic effect of hydrogen addition on ethylene jet flames in a hot and diluted coflow. Int J Hydrogen Energy 2015;40:16634–48.

[24] Medwell PR, Kalt PA, Dally BB. Imaging of diluted turbulent ethylene flames stabilized on a jet in hot coflow (JHC) burner. Combust Flame 2008;152:100–13.

[25] https://www.flatflame.com/.

[26] Pope SB. Turbulent flows. Cambridge University Press; 2000.

[27] Tennekes H, Lumley JL. A First Course in Turbulence. Cambridge, MA: The MIT Press; 1972.

[28] Pineda DI, Paxton L, Perakis N, Wei C, Luna S, Kahouli H, et al. Carbon oxidation in turbulent premixed jet flames: A comparative experimental and numerical study of ethylene, n-heptane, and toluene. Combust Flame 2020;221:371–83.

[29] https://tnfworkshop.org/data-archives/pilotedjet/